
Proceedings Paper:
Sielicki, P.W., Rigby, S.E. and Sumelka, W. (2015) Numerical predictions of the negative phase. In: Proceedings of;. 5th International Conference on Design and Analysis of Protective Structures (DAPS15), 19-21 May 2015, Singapore.

Numerical predictions of the negative phase

Piotr W. Sielicki[1*], Samuel E. Rigby[2], Wojciech Sumelka[3]

[1*] *Institute of Structural Engineering, Poznan University of Technology, Sq. M. Sklodowskiej - Curie 5 60-965 Poznan, Poland* (piotr.sielicki@put.edu.pl)
[2] *Department of Civil & Structural Engineering University of Sheffield, Mappin Street, Sheffield, S1 3JD, UK* (sam.rigby@shef.ac.uk)
[3] *Institute of Structural Engineering, Poznan University of Technology, Sq. M. Sklodowskiej-Curie 5 60-965 Poznan, Poland* (wojciech.sumelka@put.edu.pl)

Abstract

The field of blast protective design emerged in the late 1940s and focussed mainly on large scale (nuclear) explosive loading massive structures. In these situations, positive phase effects were seen to dominate and the negative phase could effectively be ignored. Recently, however, the threat has moved to smaller scale explosives and increasingly lightweight structures. Here, the negative phase becomes important, however despite this the negative phase is often overlooked.
This research presents a numerical investigation on the negative phase, with a primary focus on an accurate numerical scheme for modelling the negative phase blast pressure. Numerical tests are performed on deformable targets to determine fully reflected blast parameters, with associated numerical modelling conducted using Abaqus/Explicit. Moreover, the failure modes are obtained for light-weight panel employing the Perzyna model for metallic materials.
The computational methods are adapted for better representation of the negative phase, including mesh refinement strategies, modelling of the explosive event and accurate description of the air behaviour. The results herein can be used to inform blast resistant designers on how to accurately model negative phase effects.

Keywords: Blast loading; Negative phase; EOS modeling

1. Introduction

The behaviour of the charge followed by the detonation and pressure wave propagation through the ambient is a complex topic. In this paper the comparison of the final failure modes are obtained for the light-weight panel structure, however, for three different descriptions of the explosive loading. The primary difference bases on the description of the negative phase on the blast pressure-time history.

The explosion phenomenon starts from the explosive detonation through the blast wave propagation and finally loads the obstacle. When the process is initiated, following the explosion at the time of arrival t_a, the pressure suddenly increases to a peak value P_{so} which exceeds the ambient pressure equals to P_0. Hence, the pressure decays to P_0 in time t_0, and again reaches $P_{\overline{so}}$ pressure in order to finally reach again the barometric value, at time $t_{\overline{0}}$. The sum of times of over and under pressures is called the duration time T. The value of P_{so} is usually referred to as the peak side-on overpressure or incident peak overpressure, see Fig. 1.

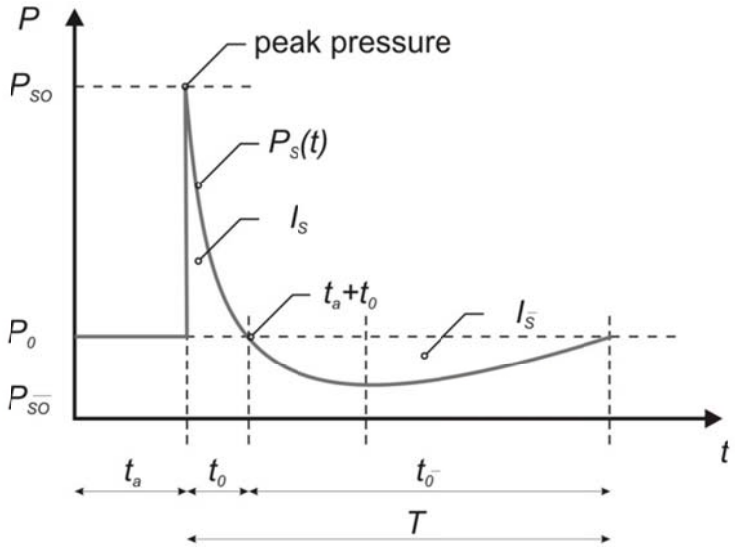

Fig. 1: Standard blast pressure as a function of time

The knowledge of the instantaneous pressure changes and the duration of the positive phase allows us to calculate the blast impulse of an explosion I_s. It is noticed that the positive phase and its impulse are highly important for the structural strength for any kind of obstacle. In fact the blast resistance capacity of any structure can be presented as lying along a curve drawn in P-I space (Sielicki 2013, UFC 2008). Moreover, considering numerically the different equations of the state it is necessary to take into account the equation for conservation of energy, see Eq.(1).

$$\rho \frac{\partial E_m}{\partial t} = (p - p_{bv}) \frac{1}{\rho} \frac{\partial \rho}{\partial t} + \mathbf{S} : \dot{\mathbf{e}} + \rho \dot{Q} \tag{1}$$

The above relation equates the increase in internal energy per unit mass E_m to the rate at which work is being done by the stresses and the rate at which heat is being added. Moreover, p is the pressure stress defined as positive in compression, p_{bv} is the pressure stress due to the bulk viscosity, $\mathbf{S}$ is the deviatoric stress tensor, $\dot{\mathbf{e}}$ is the deviatoric part of strain rate, and $\dot{Q}$ is the heat rate per unit mass. The equation of state is assumed for the pressure as a function of the current density, ρ, and the internal energy per unit mass, E_m.

The equations of the motions that are necessary to describe the blast waves of explosion are complex. It means, that it is not possible to obtain the analytical solution of spatial explosion phenomena, and that is why a numerical approach is used, i.e. finite elements modelling as a highly elaborated tool for solving blast challenges. These equations were first solved by Brode (1995) and then verified numerically by Kingery (1984). Additionally, such problems frequently incorporate the analysis of the target loading and its response. In this paper the numerical FEM analysis are performed with the use of finite elements code ABAQUS Explicit v.6.13 (Sielicki 2013, Abaqus Documentation 2012). The primary study assumes the propagation of the explosive pressure wave through a pure medium like an ambient air. Implementing the set of equations (Sielicki 2013, Belytschko et al. 2000, Eftis et al. 2003), it is possible to evaluate the problem using the following system of equations:

Equation of motion	$\sigma_{kl,l} + \rho f_k = \rho \ddot{u}_k$
Geometric equation	$\varepsilon_{kl} = 0.5\left(u_{k,l} + u_{l,k}\right)$
Equation of state	$p = p(\sigma, E_m)$
Stress boundary conditions	$\sigma_{kl} n_l = \hat{t}_k$
Displacement boundary conditions	$u_k = \hat{u}_k$
Initial conditions	$u_k = \hat{u}_k^0, \dot{u}_k = \hat{\dot{u}}_k$

(2)

where: σ_{kl} – Cauchy stress tensor component; ε_{kl} – Cauchy strain tensor component; $u_{k,l}$ – gradient of displacement component; n_l - the normal direction; $\hat{t}_k$ - traction vector; u_k, $\dot{u}_k$ - displacement and velocity components on the boundary of the body; ρ - density and E_m - specific energy. Nevertheless, Eq. (2) allows one to solve the linear dynamic problem. The nonlinear dynamic problems, which include the explosion phenomenon, must be solved with some additional modifications introduced to the set of equations Eq. (2). In this work, the solution of Eq. (2) is obtained using explicit finite element method. The widely-used Jones-Wilkins-Lee (JWL) equation of state (Sielicki 2013), as presented in Eq. (3), was used to describe the expansion of the combustion products of TNT.

$$p = A\left(1 - \frac{\omega\rho}{R_1\rho_0}\right)\exp^{\left(-R_1\frac{\rho_0}{\rho}\right)} + B\left(1 - \frac{\omega\rho}{R_2\rho_0}\right)\exp^{\left(-R_2\frac{\rho_0}{\rho}\right)} + \omega\rho E_m. \tag{3}$$

The JWL equations describe the pressure generated by chemical energy of the condensed explosive. The constitutive properties: A, B, R_1, R_2, are only available thanks to laboratory testing. E_m is the internal specific energy per unit mass and ρ is the instantaneous density of the detonation products. The initial ratio of ρ to ρ_0 used in the JWL equation is assumed to be unity. In Table 1, the properties for the TNT and ambient domains are presented. Moreover, to reach the Eq. (1) it is necessary to derive the corresponding derivatives, see Eq. (4) and Eq. (5):

$$\frac{\partial p}{\partial \rho} = \left(R_1\rho_0\frac{1}{\rho^2} - \frac{\omega}{R_1\rho_0} - \frac{\omega}{\rho}\right)A \cdot exp^{\left(-R_1\frac{\rho_0}{\rho}\right)} + \left(R_2\rho_0\frac{1}{\rho^2} - \frac{\omega}{R_2\rho_0} - \frac{\omega}{\rho}\right)B \cdot exp^{\left(-R_2\frac{\rho_0}{\rho}\right)} + \omega E_m, \tag{4}$$

$$\frac{\partial p}{\partial E_m} = \omega\rho. \tag{5}$$

The ambient air was modelled as an ideal gas (IG), see Eq. (8):

$$\begin{cases} p + p_a = (\gamma - 1)\rho E_m \\ p + p_a = \rho R(T - T^z) \end{cases} \tag{8}$$

Moreover, these relations depend on the specific internal energy E_m. In order to most accurately reflect the reality the air must be initialised with both: greater than zero internal energy as well as an initial ambient pressure. The following equations, with $\gamma = 1.4$, are used for the ideal diatomic gas modelling. The p_a is the ambient pressure, ρ is initial air density, R is the universal gas constant, and T^z is the absolute zero on the temperature scale being used. The value of the ambient pressure is represented by the sea level pressure.
The important material parameter is the specific energy, as presented in Eq. (9), which changes depending on the temperature and can be expressed in the following equation:

$$E_m = \int_0^{T-T^z} c_v(T)dT + \int_{T_0-T^z}^{T-T^z} c_v(T)dT, \tag{9}$$

where the first part is called the initial specific energy E_{m0}. There is the initial specific energy at room temperature T_0 and c_v is the specific heat at constant volume. This discretisation of the surrounding air is very important while the material model includes the principles presented in Eq. (2). The critical size of Eulerian finite elements is fixed and it equals 0.005 m. These assumptions were adopted for the two following domains: ambient air and charge domains.

Table 1: Material property for TNT and air mediums (Sielicki 2013)

JWL properties for TNT Explosive

A	3.4×10^{11}	Pa
B	3.75×10^{9}	Pa
R_1	4.15	$-$
R_2	0.9	$-$
E_m	4.2×10^{6}	$J \times kg^{-1}$
ω	0.35	$-$
C_d	6930	$m \times s^{-1}$
ρ_0	1630	$kg \times m^{-3}$
IG properties for Ambient Air		
R	287	$J \times (kg \times \mathrm{K})^{-1}$
ρ	1.297	$kg \times m^{-3}$
p_a	101325	Pa
E_m	0.193×10^{6}	$J \times kg^{-1}$
T^z	0	K
T_0	288.4	K
c_v	717.6	$J \times (kg \times \mathrm{K})^{-1}$

Solving the above equation system numerically it is possible to obtain a reliable results of the pressure-time history followed by the load distribution on the obstacle.

2. Blast Loading

2.1 Positive phase

The typical model of the blast loading is similar to Fig. 2a which bases on the experimental results. The explosion of 6kg of TNT in 1.5 stand-off. Nevertheless, during the preliminary study the authors loaded the structure only by the positive phase according to the Figs. 2b and 2c.

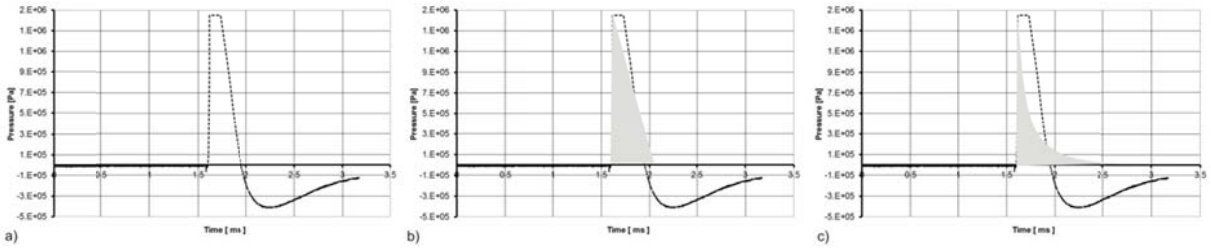

Fig. 2: Overpressure loading: a) Actual result, b) Triangle simplification, c) Logarithmic simplification

2.2 Negative phase

As mentioned previously, a full pressure-time history includes overpressure and under-pressure. This is the reason, according the title of the paper, to take into account the second loading phase. The authors introduced four different shape of the negative phase, however, preserving constant negative impulse values, see Fig. 3.

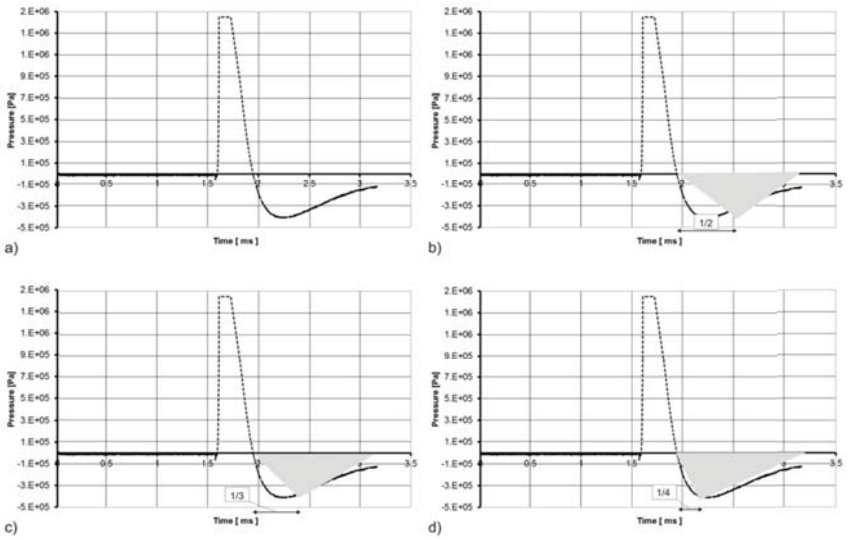

Fig. 3: Negative phases: a) Actual results, b) Triangular 1/2 simplification, c) Triangular 1/3 simplification, d) Triangular 1/4 simplification.

3. Metallic obstacle behaviour

Explosive loading induces thermomechanical process in the obstacle (Sumelka et al. 2013). This process is highly rapid in time, and is considerably influenced by wave effects (Lodygowski et al. 2012). To describe the behaviour of the obstacle within the continuum mechanics framework we obtain complex models, with huge number of material parameters (Eftis 2003, Lodygowski et al. 2013, Sumelka et al. 2013). It is clear, that identification/calibration of such models needs many sophisticated experimental tests under different loading rates, and temperatures levels (Neat-Nasser et al. 2003, Neat-Nasser et al. 2005, Mocko et al. 2013).

As mentioned, in this paper the metallic obstacle is modelled in the framework of Perzyna's type viscoplasticy accounting for anisotropic damage description. It is important to emphasise that although Perzyna model is commonly associated with famous definition of rate of viscoplastic strains in terms of overstress function only, in its present form belongs to most general and elegant formulations in mechanics (Perzyna 2008, Glema et al. 2009). One can point out at least the following original features: (i) invariance with respect to any diffeomorphism (covariant material model) (Sumelka 2013), (ii) well-posedness of evolution problem, (iii) sensitivity to the rate of deformation, (iv) finite elasto-viscoplastic deformations, (v) plastic non-normality, (vi) dissipation effects (anisotropic description of damage) (Sumelka et al. 2011), (vii) thermo-mechanical couplings (viii) length scale sensitivity are included. On the other hand, it is important that the viscoplasticity theory, being a physical one, has a deep physical interpretation derived from the analysis of a single crystal and a polycrislal behaviour (Perzyna 2005).

The evolution problem is described by the following governing equations (for comprehensive study the reader should follow recent papers in the subject cf. (Sumelka et al. 2013):

find φ as function of t and $\mathbf{x}$ satisfying.

$$\left.\begin{array}{ll} \text{(i)} & \dot{\varphi} = A(t,\varphi)\varphi + \mathbf{f}(t,\varphi); \\ \text{(ii)} & \varphi(0) = \varphi^0(\mathbf{x}); \\ \text{(iii)} & \text{The boundary conditions;} \end{array}\right\} \tag{10}$$

where φ is the unknown vector, $A(t,\varphi)$ is a spatial linear differential operator depending on t and φ, $\mathbf{f}$ is a nonlinear function, and the dot denotes the material derivative. In Eq. (10) we have $\varphi = [\upsilon \ \rho \ \tau \ \xi \ \ \vartheta]^T$,

$$\mathbf{f}=\begin{bmatrix} 0 \\ 0 \\ -\dfrac{\left\langle \Phi(\frac{f}{\kappa}-1)\right\rangle}{T_m}\left[\left(L^e+\dfrac{\chi^*\tau}{\rho_{Ref}}L^{th}+\mathbf{g}\tau+\tau\mathbf{g}+W\right):\mathbf{P}\right]-\dfrac{\chi^{**}\Xi}{\rho_{Ref}}L^{th} \\ \Xi \\ \dfrac{1}{T_m}\left\langle \Phi(\dfrac{f}{\kappa}-1)\right\rangle\dfrac{\chi^*}{\rho_{Ref}}L^{th}\tau:\mathbf{P}+\dfrac{\chi^{**}}{\rho_{Ref}}\Xi \end{bmatrix},$$

$$A=\begin{bmatrix} 0 & 0 & \dfrac{\tau}{\rho_{Ref}\rho}\text{grad} & \dfrac{1}{\rho_{Ref}}\text{div} & 0 \\ 0 & -\rho\text{div} & 0 & 0 & 0 \\ 0 & IE:\text{sym}\dfrac{\partial}{\partial\mathbf{x}}+2\text{sym}(\tau:\dfrac{\partial}{\partial\mathbf{x}}) & 0 & 0 & 0 \\ 0 & 0 & 0 & 0 & 0 \\ 0 & \dfrac{\vartheta}{c_p\rho_{Ref}}\dfrac{\partial\tau}{\partial\vartheta}:\text{sym}\dfrac{\partial}{\partial\mathbf{x}} & 0 & 0 & 0 \end{bmatrix}.$$

and $IE=L^e-\dfrac{\vartheta}{c_p\rho_{Ref}}L^{th}\dfrac{\partial\tau}{\partial\vartheta}$,

other denotes: υ is a material point velocity, ρ is a current density, τ is a Kirchhoff stress tensor, ξ is a damage variable, q is a temperature, Φ is an overstress function, f is a yield function, κ is a work hardening-softening function, T_m is a relaxation time, L^e is a stiffness tensor, χ^* and χ^{**} are irreversibility coefficients, ρ_{Ref} is a reference density, L^{th} is a thermal tensor, **g** is a metric tensor, **P** is a direction of a viscoplastic flow, and c_p denotes a specific heat.
The material properties for the 18G2A steel are presented in Table 2.

Table 2: Material property for 18G2A steel

Material parameters for 18G2A steel			
$\lambda = 121.154$ GPa	$\mu = 80.769$ GPa	$\rho_{Ref} = 7800$ kg/m^3	$m_{md} = 1$
$c = 0.067$	$b_1 = 0.02$	$b_2 = 0.5$	$b_3 = 0$
$\xi^{F*} = 0.33$	$\xi^{F**} = 0$	$m_F -$	$\|\|\mathrm{L}_{\boldsymbol{\upsilon}}\boldsymbol{\xi}_c\|\| - \mathrm{s}^{-1}$
$\delta^* = 5.6$	$\delta^{**} = 1.26$	$T_m = 2.5\ \mu$s	$m_{pl} = 0.14$
$\kappa_s^* = 342$ MPa	$\kappa_s^{**} = 77$ MPa	$\kappa_0^* = 274$ MPa	$\kappa_0^{**} = 62$ MPa
$\beta^* = 11.0$	$\beta^{**} = 2.5$	$n_1 = 0$	$n_2 = 0.25$
$\chi^* = 0.8$	$\chi^{**} = 0.1$	$\theta = 10^{-6}$ K^{-1}	$c_p = 470$ J/kgK

4. Numerical example

The authors computed the light panel structure, according to Fig. 4, however, for a different loading conditions. Three take into account only the positive phase. Moreover, another four the positive phase – base on the actual results – and negative phases in addition. Nevertheless, the shapes of the negative phase were different, according to the Fig. 3.

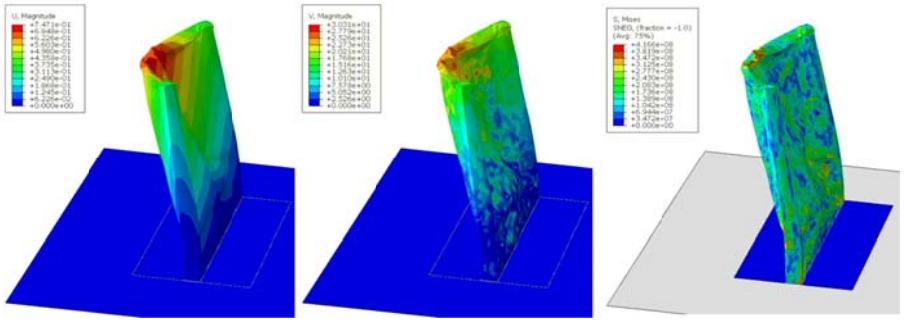

Fig. 4: Light-weight panel structure subjected to the different kinds of the negative phase loading

The numerical solution is obtained using Abaqus Explicit v.6.13. Moreover, the JWL equation was introduced by the author in VUEOS subroutine base on the Fortran coding. In the Fig. 4 the displacement, velocity and Misses stresses are presented. The main goal of this study dealt with the steel frame which is embedded inside the panel structure.

5. Conclusions

A series of numerical experiments were conducted where different loading description of the negative phase were used. All results were obtained for 6kg of TNT box charge in 1.5m stand-off. The authors presented the failure of the metallic structure under blast wave action. Furthermore, this failure strictly depends on the loading conditions which are applied. The introducing the negative phases influences strongly on the deformation mode followed by failure of the obstacle. This is an important feature especially for the lightweight structures. This outcome was proved in series on FEM examples.

Acknowledgements

This work is supported by the Polish National Centre for Research and Development (NCBiR) under Grant UOD-DEM-1-203/001.

References

[1] Abaqus 6.13. Documentation Collection. (2012).

[2] Belytschko Ted, Liu W.K., and Moran B. (2000), Nonlinear finite elements for continua and structures. *Wiley*.

[3] Brode H.L. (1995), Numerical Solutions of Spherical BlastWaves. Defense *Technical Information Center*.

[4] Departments of the army US Army Manual (2008). Design and Analysis of Hardened Structures to Conventional Weapons Effects. UFC 3-340-01.

[5] Eftis J., Carrasco C., and Osegueda R.A.. A constitutive-microdamage model to simulate hypervelocity projectile-target impact, material damage and fracture. International Journal of Plasticity, 19:1321–1354, 2003.

[6] Glema A., Łodygowski T., Perzyna P., Sumelka W. (2009) The Numerical Analysis of the Intrinsic Anisotropic Microdamage Evolution in Elasto-Viscoplastic Solids International Journal of Damage Mechanics, 18, 3, pp. 205-231.

[7] Kingery C.N. and Bulmash G. (1984) Airblast parameters from TNT spherical air burst and hemispherical surface burst. Ballistic Research Laboratory.

[8] Lee E, Finger M, Collins W. (1973) JWL equation of state coefficients for high explosives. Rept-UCID-16189, Lawrence Livermore National Laboratory.

[9] Łodygowski T., Rusinek A., Jankowiak T., Sumelka W. (2012), Selected topics of high speed machining analysis, Engineering Transactions, 60, 1, pp. 69-96.

[10] Łodygowski T., Sumelka W. (2012), Damage Induced by Viscoplasitc Waves Interaction, Vibrations in Physical Systems, pp. 23-32, vol. 25.

[11] Moćko W. and Kowalewski Z.L. (2013) Application of fem in the assessment of phenomena associated with dynamic investigations on a miniaturised ict testing stand. Kovove Materialy-Metallic Materials, 51:71–82.
[12] Nemat-Nasser S. and Guo W.-G. (2003) Thermomechanical response of DH-36 steel plates over a wide range of strain rates and temperatures. Mechanics of Materials, 35 :1023–1047.
[13] Nemat-Nasser S. and Guo W.-G. (2005) Thermomechanical response of HSLA-65 steel plates: experiments and modeling. Mechanics of Materials, 37:379–405.
[14] Perzyna P. (2005) The thermodynamical theory of elasto-viscoplasticity. Engineering Transactions, 53 :235–316.
[15] Perzyna P. (2008) The thermodynamical theory of elasto-viscoplasticity accounting for microshear banding and induced anisotropy effects. Mechanics,27 (1):25–42.
[16] Sielicki, P.W. (2013) Masonry Failure under Unusual Impulse Loading. Publishing House of Poznan, University of Technology, ISBN 978-83-7775-274-6, Poznan.
[17] Sumelka W., Łodygowski T. (2013), Reduction of the number of material parameters by ANN approximation, Computational Mechanics, 52, 2, pp. 287-300.
[18] Sumelka W., Łodygowski T. (2013) Thermal stresses in metallic materials due to extreme loading conditions, ASME Journal of Engineering Materials and Technology, 135, 2, pp. 021009-1-8.
[19] Sumelka W. (2013), Role of Covariance in Continuum Damage Mechanics, ASCE Journal of Engineering Mechanics, 139, 11, pp. 1610-1620
[20] Sumelka W., Łodygowski T. (2011) The influence of the initial microdamage anisotropy on macrodamage mode during extremely fast thermomechanical processes, Archive of Applied Mechanics, 81, 12, pp. 1973-1992
[21] Wlodarczyk, E. (1993), Modyfication of the JWL equation of state – the W equation of state, Journal of Technical *Physics*, 34,3.